# Asymmetric Electrostatic and Hydrophobic–Hydrophilic Interaction Forces between Mica Surfaces and Silicone Polymer Thin Films

**Stephen H. Donaldson, Jr.,[†] Saurabh Das,[†] Matthew A. Gebbie,[‡] Michael Rapp,[†] Louis C. Jones,[†] Yuri Roiter,[§] Peter H. Koenig,[⊥] Yonas Gizaw,[§] and Jacob N. Israelachvili[†,‡,*]**

[†]Department of Chemical Engineering, University of California, Santa Barbara (UCSB), Santa Barbara, California 93106-5080, United States, [‡]Materials Department, University of California, Santa Barbara (UCSB), Santa Barbara, California 93106-5050, United States, [§]The Procter & Gamble Co., Winton Hill Business Center, 6210 Center Hill Avenue, Cincinnati, Ohio 45224, United States, and [⊥]The Procter & Gamble Co., Modeling and Simulation/Computational Chemistry, 8611 Beckett Road, West Chester, Ohio 45069, United States

**ABSTRACT** We have synthesized model hydrophobic silicone thin films on gold surfaces by a two-step covalent grafting procedure. An amino-functionalized gold surface reacts with monoepoxy-terminated polydimethylsiloxane (PDMS) *via* a click reaction, resulting in a covalently attached nanoscale thin film of PDMS, and the click chemistry synthesis route provides great selectivity, reproducibility, and stability in the resulting model hydrophobic silicone thin films. The asymmetric interaction forces between the PDMS thin films and mica surfaces were measured with the surface forces apparatus in aqueous sodium chloride solutions. At an acidic pH of 3, attractive interactions are measured, resulting in instabilities during both approach (jump-in) and separation (jump-out from adhesive contact). Quantitative analysis of the results indicates that the Derjaguin–Landau–Verwey–Overbeek theory alone, *i.e.*, the combination of electrostatic repulsion and van der Waals attraction, cannot fully describe the measured forces and that the additional measured adhesion is likely due to hydrophobic interactions. The surface interactions are highly pH-dependent, and a basic pH of 10 results in fully repulsive interactions at all distances, due to repulsive electrostatic and steric-hydration interactions, indicating that the PDMS is negatively charged at high pH. We describe an interaction potential with a parameter, known as the Hydra parameter, that can account for the extra attraction (low pH) due to hydrophobicity as well as the extra repulsion (high pH) due to hydrophilic (steric-hydration) interactions. The interaction potential is general and provides a quantitative measure of interfacial hydrophobicity/hydrophilicity for any set of interacting surfaces in aqueous solution.

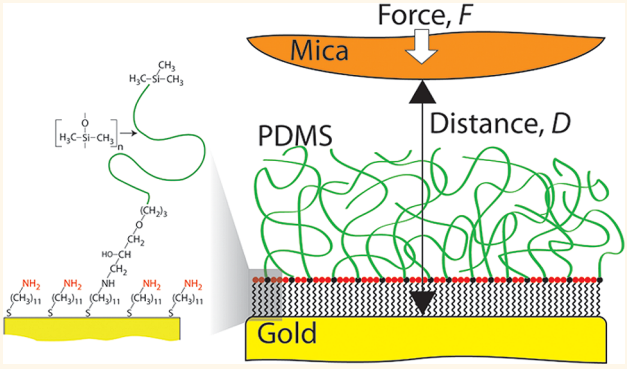


**KEYWORDS:** hydrophobic · hydrophilic · click reaction · PDMS monolayer · mica · thin film

The physical and chemical properties of silicones (high thermal stability, low conductivity, low toxicity, biocompatibility, hydrophobicity, low chemical reactivity) have led to widespread use in many materials, including in lubricants,[1,2] microfluidic devices,[3−6] biomedical devices and implants,[6−8] and emulsions.[9−11] In many of these applications, the interfacial properties of silicone (*e.g.*, surface energy, hydrophobicity) and the physical interactions of silicone with other materials (*e.g.*, adhesion, adsorption, hydrophobic interactions, steric interactions, electrostatic interactions) are key determining factors for obtaining the desired behavior and functionality.

For example, interactions between biofilms and silicone interfaces determine the biocompatibility of medical and cosmetic implants.[8] The wetting behavior and chemical structure of silicones can be modified by chemical treatments,[12] making the silicone more suitable for microfluidic electrophoresis and allowing for covalent attachment of DNA molecules in microfluidic biosensors.[13] Hydrophobicity and other interfacial properties of silicone also influence the adsorption of surfactants and other

* Address correspondence to jacob@engineering.ucsb.edu.

Received for review August 13, 2013 and accepted October 19, 2013.

**Published online October 19, 2013**
**10.1021/nn4050112**

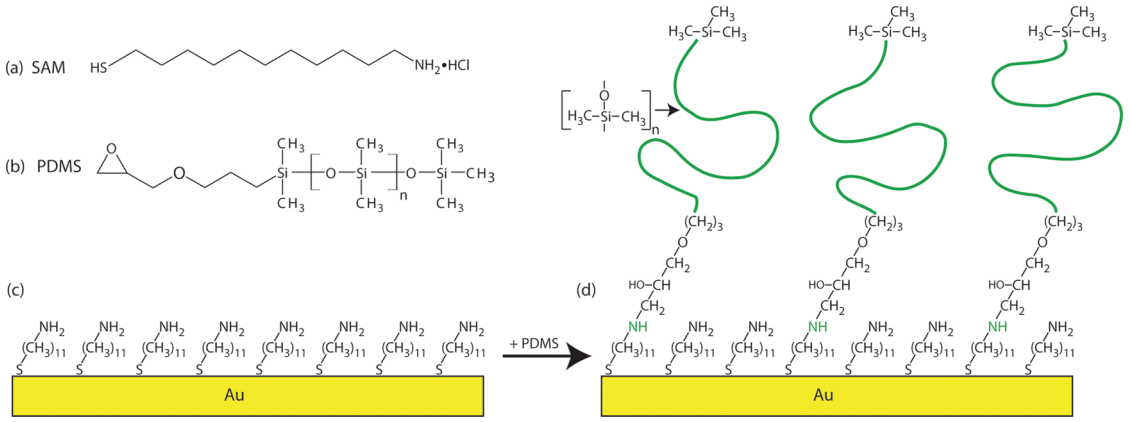


**Figure 1. Chemical structures of the materials and films used in this study. The raw materials include (a) 11-amino-1-undecanethiol hydrochloride (SAM) and (b) monoglycidyl ether-terminated poly(dimethylsiloxane) (PDMS), where the number of monomer units (*N*) = 64. The initial functionalization utilizes thiol chemistry to form the $NH_2$-SAM shown in (c). Immersing the $NH_2$-SAM into the pure PDMS liquid and heating at 130 °C for 1 h results in the covalently attached thin silicone film shown in (d).**

small molecules, which in turn determines the phase behavior of emulsions,[9,10] and can impact the measurement of tiny chemical concentrations in microfluidics experiments.[14]

In this work, we have synthesized covalently grafted thin films of polydimethylsiloxane (PDMS) on molecularly smooth gold surfaces to design a model silicone surface. The wetting properties were examined by contact angle measurements, while the surface chemistry at the PDMS surface was determined using X-ray photoelectron spectroscopy (XPS). The main goal of this study was to determine the magnitude and range of the interaction forces (*i.e.*, van der Waals, electrostatic, hydrophobic, steric, polymeric) between PDMS and a mineral surface. The asymmetric interaction forces were directly measured between the PDMS surface and an apposing mica surface with the surface forces apparatus (SFA). The surface properties of mica are well-known, so the silicone–mica model system allows for complete determination of the interfacial properties and interactions of silicone surfaces.

The PDMS surfaces were synthesized using a two-step grafting procedure by thiol and click chemistry, as summarized in Figure 1. A molecularly smooth gold surface was functionalized with an amine-terminated thiol self-assembled monolayer (Figure 1a, $NH_2$-SAM). Monoglycidyl ether terminated PDMS (Figure 1b) was reacted with the $NH_2$-SAM, a typical example of a click reaction,[15,16] to give the amino-alcohol chemical structure shown in Figure 1c. This synthesis procedure forms a stable, smooth, hydrophobic, covalently attached nanothin film of PDMS (Figure 1d). Similar graft-to strategies have been used for forming functional monolayers by click chemistry for antibiofouling,[17] stem-cell adhesion,[18] and biocatalysis studies.[19]

The silicone monolayers provide a model system for determining the asymmetric interactions between hydrophobic and hydrophilic surfaces, which remains an open issue both experimentally and theoretically. Many of the previous force measurements between hydrophobic and hydrophilic surfaces were done with AFM,[20,21] which lacks the absolute distance measurement of the SFA, or involved physically adsorbed surfactants that exhibit subtle electrostatic effects.[22] While polystyrene films were prepared by a similar graft-to procedure,[23,24] force measurements between the PS films and mica surfaces were not reported. Studies between liquid silicone films and mica surfaces have been done with AFM,[25,26] but the liquid film adds additional complexity due to hydrodynamic interactions.

The silicone–mica system described here utilizes two inherently stable surfaces and allows for unambiguous insights into the interaction potential and specifically the separate electrostatic, hydrophobic, and steric contributions between silicone and mica surfaces. We have measured the interactions between silicone and mica surfaces as a function of solution pH and electrolyte concentration, allowing for insights into hydrophobic and hydrophilic interactions, as well as ion adsorption at PDMS interfaces that can modify both the adhesive and long-range interactions between silicone and mica surfaces.

## RESULTS AND DISCUSSION

**Preparation and Characterization of Silicone Thin Films on Extended Gold Surfaces.** Stable, hydrophobic PDMS surfaces were prepared using the two-step grafting procedure shown in Figure 1. As described in more detail in the Methods section, a molecularly smooth gold surface was immersed in a 1 mM ethanolic solution of 11-amino-1-undecanethiol (chemical structure shown in Figure 1a) for 2 h. As shown in Figure 1c, this initial functionalization results in the $NH_2$-SAM. Following the $NH_2$-SAM formation, the surface was immersed in monoglycidyl ether terminated PDMS liquid (monomer structure shown in Figure 1b) and heated to 130 °C for 1 h. The

terminal glycidyl ether group undergoes a nucleophilic ring-opening by the terminal amine on the pregrafted monolayer, resulting in the amino−alcohol linkage between the $NH_2$-SAM and PDMS shown in Figure 1d.

We performed several measurements to confirm the successful attachment of PDMS at the $NH_2$-SAM surface. First, the advancing and receding contact angle of water droplets on these PDMS surfaces were measured, which show a very high contact angle on advancing ($\theta_a = 113° \pm 2°$) and only a small degree of hysteresis upon receding ($\theta_r = 103° \pm 2°$). The slightly lower contact angle during receding is likely due to small rearrangements of interdigitated PDMS chains and interfacial water. This small degree of hysteresis indicates that molecular detachment of grafted PDMS does not occur, and no contact line pinning was observed, indicative of a very smooth film with few underlying microscopic defects.

The proposed surface chemistry between gold, $NH_2$-SAM, and PDMS was established using XPS. Thiol samples were prepared using the standard 2 h preparation (thiol 2), as well as an overnight preparation for 17 h (thiol 17). The PDMS film was prepared as described in the Methods section. A summary of the XPS results for these three samples is shown in Figure 2. The N 1s region shows three distinct peaks, all of which correspond to distinct chemical species. For the 2 h thiol (black curve), two peaks are observed near 399.6 and 401.7 eV, corresponding to the primary amine peak for the SAM, as well as a protonated amine peak, respectively. The protonated peak becomes much larger than the primary amine peak for the 17 h preparation (red curve), indicating that the quality of the $NH_2$-SAM decreases for longer preparation times. After PDMS attachment (confirmed also *via* the Si 2s signal shown in the inset) to the $NH_2$-SAM, a new prominent N 1s peak at 400.4 eV is observed (green curve) that corresponds to a secondary amine formed upon reaction of the primary amine with the terminally functionalized PDMS. The N 1s peak shift to higher binding energy after reaction confirms that a covalent bond is formed, likely between the terminal amine on the $NH_2$-SAM and the terminal glycidyl ether on the PDMS. The Si 2s signal shown in the Figure 2 inset shows no signal before the PDMS treatment, indicating that there is a negligible amount of silicon present in the two thiol monolayers (thiol 2 and thiol 17, red and black curves, Figure 2 inset). After PDMS treatment, a large peak is observed in the Si 2s region, providing further confirmation of the silicone attachment.

Measurement of the wetting properties and surface chemistry of the PDMS surface indicates that the grafting procedure results in a very hydrophobic, stable thin film of PDMS on extended gold surfaces. As described below, the exact thickness of the film, along with interaction force profiles, was measured with the SFA to fully characterize the interaction forces

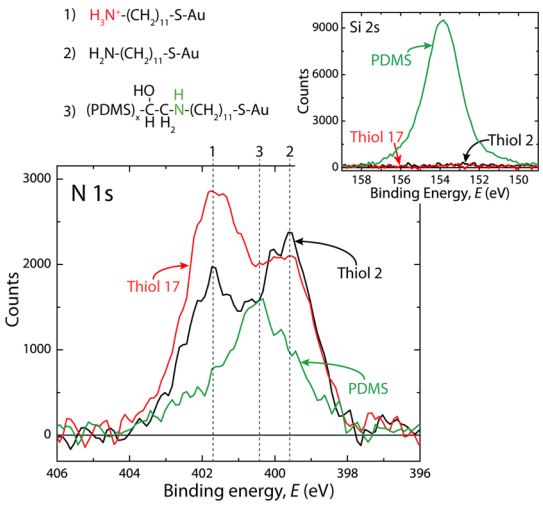


**Figure 2. High-resolution N 1s and Si 2s X-ray photoelectron spectra of amine-terminated thiol self-assembled monolayers on gold and as-synthesized PDMS thin films on gold (see text for details) in the N 1s and Si 2s regions. The peaks labeled "1", "2", and "3" correspond to the amine structures drawn in the top left, *i.e.*, protonated amine, primary amine, and secondary amine. Two thiol preparation times were examined, by immersing the gold surface in thiol solution for 2 h (black curve, "thiol 2") and 17 h (red curve, "thiol 17"). Deactivation (protonation) of the amine terminal group is observed for longer thiol preparations. A distinct shift in the N 1s spectrum is observed after PDMS attachment (green curve), indicating successful covalent linkage of the PDMS molecule to the terminal amine group. As shown in the inset, a large peak in the Si 2s region is observed after PDMS attachment, while no signal is observed in the Si 2s region for the thiol 2 and thiol 17 samples because the amount of silicon present in those samples is negligible.**

between PDMS and mica surface. To examine the effects of salt concentration and pH on the electrostatic double-layer forces, force measurements were performed in sodium chloride aqueous solutions of varying salt concentration (1, 5, and 10 mM NaCl) at pH ~3 and pH ~10.

**Thickness Measurements of Silicone Thin Films by FECO.** Measurements of the wetting properties showed very hydrophobic contact angles for the silicone films, indicating that the PDMS polymer chains fully cover the underlying surface. The conformation of polymeric chains grafted to surfaces is largely determined by the solvent quality and the grafting density.[27] As the measurements here are concerned with behavior of silicones in aqueous solutions, we focus on polymeric behavior in poor solvents. In a poor solvent at low grafting density, the polymer chains collapse and aggregate, resulting in surface "micelles" of polymer chains.[28] Conversely, at moderate to high grafting density, the chains' excluded volume prevents full collapse and only weak collapse occurs, in which the chains are still somewhat extended and the layer thickness depends only on the polymer length (number of monomer units, *N*, per polymer chain).[28,29] As indicated by an AFM topography scan of the silicone film in air (see Supporting Information for more details), the surface

topography is flat with a roughness of ±4 Å, indicating that the chains have not phase separated or aggregated and that the PDMS chains are within the moderate-to-high grafting density regime. To gain quantitative information about the film structure and polymer chain conformation within the PDMS film, we measured the film thickness of the silicone by the fringes of equal chromatic order (FECO) optical technique.

In air, the PDMS chains collapse due to van der Waals interactions, and the film thickness, $T_{PDMS}$, can be measured in order to determine the grafting density by eq 1, where $M_n$ = 5000 g/mol is the number average molecular weight, $N_A$ is Avogadro's number, $\rho = 0.965$ g/mL is the bulk PDMS density, and $\Gamma$ is the grafting density. This calculation assumes a uniform density throughout the film.

$$\Gamma = \rho N_A T_{PDMS}/M_n \quad (1)$$

We measured the film thickness in air for several independently prepared samples and several different contact points on each sample. The measurement by FECO in air gave a thickness $T = 3 \pm 1$ nm, giving an average grafting density $\Gamma = 3.5 \times 10^{17}$ molecules/m$^2$. Assuming an area per molecule of about 28 Å$^2$ for the $NH_2$-SAM indicates that about 10% of the sites on the $NH_2$-SAM are occupied by a PDMS molecule. Furthermore, the distance between grafting sites, $s = 1.7$ nm where $\Gamma = 1/s^2$, is less than the radius of gyration of the polymer ($R_g \approx 2.6$ nm, calculated for a theta solvent by $R_g = aN^{1/2}$, where $a = 0.364$ nm is the monomer segment length and $N = 64$ is the number of monomer units), providing confirmation that the grafting density is high and the interfacial polymers are in the brush regime. We also estimated the grafting density by fitting the XPS peaks, as shown in the Supporting Information, which indicates that about 30% of $NH_2$-SAM sites are occupied. We consider the SFA thickness measurement to be more quantitative, but 30% is within the observed range of values from the SFA measurements and provides an upper bound.

Although water is a poor solvent for PDMS, the film swells in aqueous solution to a measured value of $T_{PDMS} = 6 \pm 2$ nm. Water is relatively insoluble in bulk PDMS, so this is likely a surface effect where some water and/or ions can penetrate into the interfacial region. The van der Waals interactions between the chains are weaker in water than in air, and the PDMS interface has a relatively low grafting density, possibly allowing more space for water or ion penetration upon introduction to water. As shown below, ion adsorption plays a big role at PDMS interfaces, so ion penetration into the layer is possible. These combined factors lead to a slightly swelled film in aqueous solution.

**Interaction Forces between PDMS and Mica Surfaces: Acidic pH.** To determine the surface properties and interaction forces of the PDMS surface, the interactions between PDMS and a mica surface were directly measured by SFA. The experimental setup is shown in Figure 3, in which a freshly prepared PDMS surface

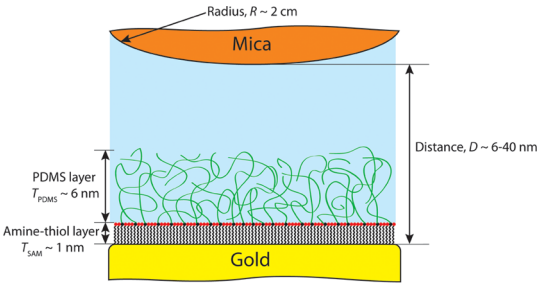


**Figure 3. Experimental setup in the surface forces apparatus (SFA) measurements performed in this study. Force measurements were performed between a PDMS thin film, prepared as described above, and a clean mica surface in sodium chloride solutions (1, 5, and 10 mM NaCl at pH 3 and pH 10).**

on gold faces an apposing mica surface in the SFA. In these experiments, the force, $F$, was measured as a function of distance, $D$, where $D = 0$ is defined at flat molecular contact between the mica surface and a clean gold surface in air. The absolute thickness of the PDMS was determined in each experiment by compressing the PDMS to very high load ($F/R > 500$ mN/m) against the mica surface. A flat, smooth contact was established in every case, resulting in a thickness $T_{PDMS} = 6 \pm 2$ nm. The error represents variation over at least 10 separate experiments; the thickness of a single freshly prepared surface, as determined by measuring at least three independent contact positions, varies only by ±0.5 nm, corresponding well with the roughness of the PDMS as measured by AFM (root mean squared roughness ~0.4 nm).

The interaction forces between the PDMS and a mica surface at low pH are shown in Figure 4. Adhesive forces are measured during both approach and separation, with a small jump-in on approach and jump-out on separation. The average adhesion force decreases slightly from 5.5 ± 2 mN/m to 1.7 ± 0.6 mN/m as the salt concentration increases from 1 mM to 10 mM NaCl. According to previous work, and our own experiments with mica surfaces shown in the Supporting Information, the mica is weakly charged at this pH,[30,31] resulting in an electrostatic double layer interaction. However, as shown in detail below, the Derjaguin–Landau–Verwey–Overbeek (DLVO) theory alone does not account for the measured adhesion, and it is likely that the adhesion is due to weak hydrophobic attraction between the very hydrophobic PDMS and the low charge density mica.

We previously derived an interaction potential for the hydrophobic interaction between stressed surfactant bilayers,[32] which we found depends on the amount of stressed area per molecule $a$, over and above the equilibrium area per molecule $a_0$, as shown in eq 2a, where $W_H$ is the hydrophobic interaction energy per unit area between flat surfaces, $\gamma$ is the hydrophobic–water interfacial tension, and $D_H$ is the decay length of the hydrophobic interaction ($D_H \approx$ 1 nm for extended surfaces). In eq 2a, when $a = a_0$,

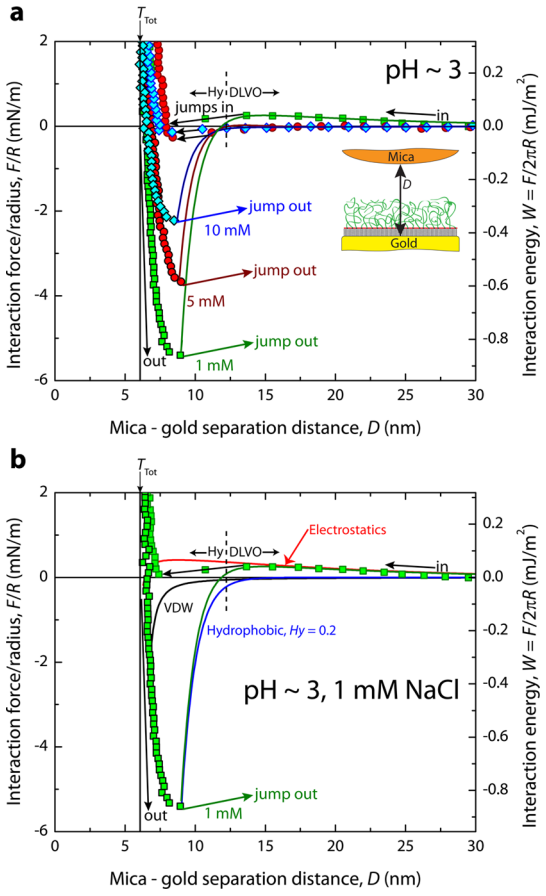


**Figure 4. (a) Force runs measured by SFA between grafted PDMS and mica surfaces. Experiments performed in aqueous salt solution at pH ~3 and sodium chloride concentrations of 1, 5, and 10 mM. A jump-in is observed for each salt concentration, at which point the gradient of the force profile is larger than the spring constant. The jump-in point is indicated by a black arrow on the curves. (b) Same data as above for 1 mM NaCl only, displaying the separate contributions to the overall force curve (green curve), as calculated by eq 3. This example shows the necessity of including a contribution from the hydrophobic interaction to account for the measured adhesion. The dotted line demarcates a critical distance: at larger distances the forces are dominated by long-range electrostatic interactions (indicated by the "DLVO" label), while at smaller distances the forces are dominated by short-range hydrophobic forces (indicated by the "Hy" label).**

there is no contribution from the hydrophobic interaction. However, as the bilayers are stressed, $a$ becomes greater than $a_0$ and the hydrophobic interaction progressively contributes a stronger attractive interaction. When $a \gg a_0$, the bilayers are fully stressed and the maximum hydrophobic interaction is obtained.

$$W_H = -2\gamma(1 - a_0/a)e^{-D/D_H} \quad (2a)$$

$$W_H = -2\gamma(1 - f)e^{-D/D_H} \quad (2b)$$

$$W_H = -2\gamma Hy\, e^{-D/D_H} \quad (2c)$$

We generalized eq 2a further, to the form shown in eq 2b, in order to account for polystyrene-coated nanoparticle aggregation as a function of changing solvent quality,[33] where $f \equiv a_0/a$ and can be thought of as the area ratio of hydrophilic to hydrophobic area at an interface. When $f = 1$, there is no additional contribution from hydrophobic or hydrophilic interactions, while $0 < f < 1$ corresponds to progressively increasing hydrophobic interactions, and $f > 1$ corresponds to a repulsive hydrophilic contribution to the overall force, otherwise known as a steric-hydration force[34] and with the identical decay length $D_H \approx 1$ nm.

We now introduce a more intuitive general form of the interaction potential, as shown in eq 2c, where $Hy \equiv (1 - a_0/a)$ is termed the Hydra parameter and more intuitively corresponds to the fraction of *hydrophobic* area at an interface. Thus, $Hy = 0$ indicates zero contribution from hydrophobicity, while $Hy = 1$ indicates the maximum hydrophobic interaction. $Hy < 0$ results in an overall repulsive steric-hydration interaction generally due to adsorbed ions or hydrated species. In this way, $Hy$ in eq 2c can empirically describe the gamut of hydration-based interactions, from hydrophobic surfaces that completely dewet water to a fully hydrated surface with a contact angle of 0°. Including the hydrophobic interaction along with the van der Waals interaction and constant potential asymmetric electrostatic interaction results in the following overall interaction potential, eq 3:

$$\frac{F(D)}{R} = -\frac{1}{6}\left(\frac{A_{mPg}}{D^2} + \frac{A_{mwP}}{(D - T_{Tot})^2}\right) + 2\pi\varepsilon\varepsilon_0\kappa \times \left[\frac{2\psi_m\psi_P e^{-\kappa(D - T_{Tot})} - (\psi_m{}^2 + \psi_P^2)e^{-2\kappa(D - T_{Tot})}}{1 - e^{-2\kappa(D - T_{Tot})}}\right] - 4\pi\gamma Hy e^{-(D - T_{Tot})/D_H} \quad (3)$$

where $W_H$ was converted to $F/R$ by the Derjaguin approximation, *i.e.*, $F/R = 2\pi W$, $D$ is the absolute separation distance between mica and gold, $T_{Tot} = T_{PDMS} + T_{SAM} = 7 \pm 2$ nm is the total hard-wall thickness, $A_{mPg} = 3.4 \times 10^{-20}$ J is the Hamaker constant for mica interacting with gold across PDMS, $A_{mwP} = 7.1 \times 10^{-21}$ J is the Hamaker constant for mica interacting with PDMS across water, $\varepsilon$ is the dielectric constant of water, $\varepsilon_0$ is the vacuum permittivity, $\kappa$ is the inverse of the Debye length, and $\psi_m$ and $\psi_P$ are the surface potentials of the mica and PDMS, respectively. The Hamaker constants were calculated as described in the Supporting Information (see eqs S2 and S3), while $\kappa$ was calculated from the sodium chloride molarity, [NaCl], by eq 4:

$$\kappa = (2N_A[\mathrm{NaCl}]e^2/\varepsilon\varepsilon_0 kT)^{1/2} \quad (4)$$

where $N_A$ is Avogadro's number, $e$ is the fundamental charge, $k$ is Boltzmann's constant, and $T$ is temperature. In these measurements, all of the parameters in eq 3 are fixed except for $\psi_m$, $\psi_P$, and $Hy$. The PDMS−water interfacial tension, $\gamma$, is 44 mJ/m$^2$, while the mica surface potentials were measured in a separate experiment at pH ~3 over the same range of salt concentrations

(see Supporting Information). Thus, for these low-pH force runs only two fitting parameters were used. The long-range forces were fitted by adjusting $\psi_P$, while the short-range adhesive forces were fitted by adjusting *Hy*.

The mica and PDMS surface potentials for the low-pH measurements are shown in Table 1, along with the fitted *Hy* values. The mica surface potential stays roughly constant between −40 and −60 mV as the salt concentration is increased from 1 mM to 10 mM NaCl. Mica is well known to be a constant potential surface.[35] The surface potential, $\psi_0$, can be used to calculate the surface charge density, $\sigma$, from the Grahame equation, as shown in eq 5, where all parameters are as described for eq 4.

$$\sigma = \sqrt{8\varepsilon_0\varepsilon kT}\sinh(e\psi_0/2kT)[\mathrm{NaCl}]^{1/2} \qquad (5)$$

Even though the surface potential stays relatively constant at the mica surface, the surface charge density increases with increasing salt concentration according to eq 5, from −0.0032 C/m$^2$ at 1 mM NaCl to 0.015 C/m$^2$ at 10 mM NaCl. As might be expected for a hydrophobic surface, the PDMS surface potentials and surface charge densities are zero within the experimental error for all salt concentrations. *Hy* decreases from about 0.2 to about 0.1 as the salt concentration increases from 1 to 10 mM NaCl.

The attractive interactions, measured during both approach and separation as jumps into or out of adhesive contact, are likely due to hydrophobic interactions. The jumps are mechanical instabilities that occur when the gradient of the force−distance profile is greater than the spring constant, and thus the highly sloped regions of the force curves are impossible to access by this measuring technique.[36] However, both the jump-in and jump-out points are well described by the theoretical curves, and it is clear that the van der Waals forces are not strong enough to result in jumps-in at the measured distances (Figure 4b). Thus, a longer ranged and stronger interaction must be invoked, and the hydrophobic interaction is the most likely mechanism. This is potentially a general effect between hydrophobic films and mica surfaces at low pH: as shown in the Supporting Information, a weak hydrophobic attraction must be included also for the interactions between a covalently attached alkanethiol monolayer and a mica surface.

While *Hy* decreases slightly with increasing salt concentration, the effect is minor and the measured *Hy* values are roughly the same within experimental error. The decreasing *Hy* does not necessarily indicate that hydrophobic interactions are weaker at higher salt concentration. Rather, the *effective* hydrophobic interaction is slightly decreased due to increased hydrophilicity (increased charge density) at the mica interface. At this point, our theory is not yet equipped for asymmetric surface interactions, as in this case, where the PDMS surface likely contributes to the overall hydrophobic interaction to a greater degree than the mica surface. We expect that the interaction potential for asymmetric surface interactions would depend on the interfacial tension of each surface with water, along with an effective *Hy* for each surface, *i.e.*, $W_{H,12} = W_{H,12}(\gamma_1, \gamma_2, Hy_1, Hy_2)$, and should of course reduce to eq 2c when $\gamma = \gamma_1 = \gamma_2$ and $Hy = Hy_1 = Hy_2$.

**TABLE 1. Parameters for Modeling the Overall Interaction between PDMS Thin Films and Mica Surfaces at pH ∼3[a]**

| [NaCl] (mM) | $\kappa^{-1}$ (nm) | $\psi_m$ (mV) | $\psi_P$ (mV) | *Hy* |
|---|---|---|---|---|
| 1 | 9.7 | −40 ± 10 | −9 ± 13 | 0.18 ± 0.12 |
| 5 | 4.3 | −60 ± 10 | −6 ± 13 | 0.08 ± 0.05 |
| 10 | 3.1 | −55 ± 10 | −3 ± 5 | 0.07 ± 0.04 |

[a] The mica surface potential $\psi_m$ was measured in a separate experiment, and the Debye length ($\kappa^{-1}$) was calculated from the salt concentration, eq 4. The only fitting parameters were the PDMS surface potential ($\psi_P$) and *Hy*, which dominate at different length scales (Figure 4).

**Interaction Forces between Silicone Thin Films and Mica Surfaces: Basic pH.** The measured interaction forces between the PDMS and a clean mica surface at varying sodium chloride concentrations and pH ∼10 are shown in Figure 5. The interaction is fully repulsive and reversible at all distances during both approach and separation. The long-range repulsive force shows an exponential decay that is strongly modulated by the salt concentration, a signature behavior of electric double layer interactions. The repulsive forces can be quantitatively described at all distances by eq 3, where now a negative *Hy* value is used to describe the short-range hydration repulsion. Similar to the above analysis, the forces are dominated by electrostatics at large distances and a hydrophilic repulsion at short-range, allowing for independent fitting of the PDMS surface potential ($\psi_P$) and *Hy*. We note that these measured forces can also be described by a DLVO model using constant charge boundary conditions, and the simple constant charge DLVO model fits nearly as well as the model described here. However, we determined that the constant potential DLVO plus hydration model is more likely for the following reasons. Previous work indicates that mica tends to follow constant potential boundary conditions.[35] Furthermore, most colloidal systems are closer to constant potential, with the exception of very highly charged interfaces that are fully ionized, which does not appear to be the case for the PDMS surface.

Table 2 shows the Debye lengths and measured surface potentials for all of the salt concentrations. As expected from previous work,[35] the mica surface potential remains approximately constant for increasing salt concentration at a value of about −100 mV (see Supporting Information), while the mica surface charge density becomes more negative, going from −0.012 C/m$^2$ to −0.044 C/m$^2$ as the NaCl concentration increases from 1 mM to 10 mM. The PDMS surface potential decreases from *ca.* −100 mV to *ca.* −40 mV as the NaCl concentration increases from 1 mM to 10 mM, while the PDMS surface charge stays relatively constant

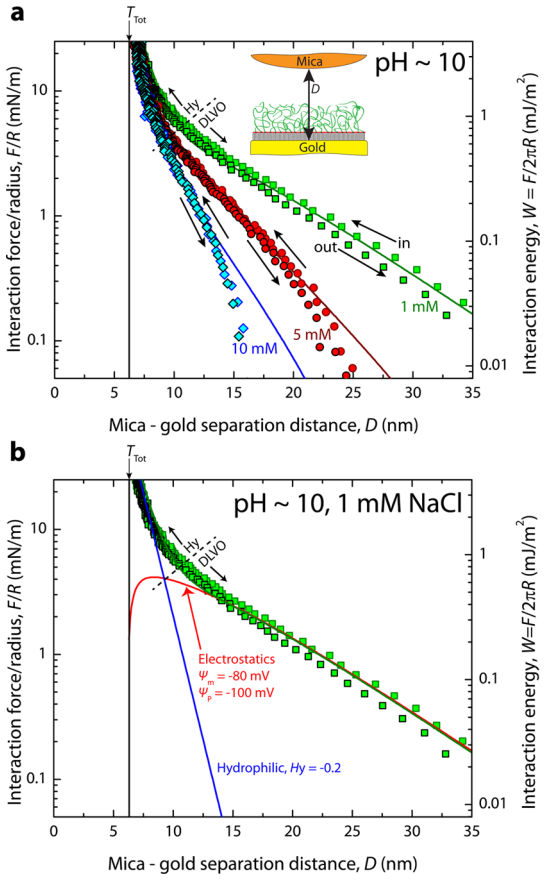


**Figure 5. (a) Force runs measured by SFA between grafted PDMS and mica surfaces for salt concentrations of 1, 5, and 10 mM NaCl at pH ~10. (b) Same data for 1 mM NaCl only, showing the separate contributions from electrostatic interactions and hydrophilic (steric-hydration) interactions. The dotted line demarcates a critical distance: at larger distances the forces are dominated by long-range electrostatic interactions (indicated by the "DLVO" label), while at smaller distances the forces are dominated by short-range hydrophilic forces (indicated by the "Hy" label).**

at $-0.013 \pm 0.003$ C/m$^2$ for all three salt concentrations. We have not observed any effects on the electrostatic forces due to the underlying $NH_2$-SAM layer. More than likely, that layer is uncharged, and water/ion penetration does not extend down to that interface, so there is no observed effect of changing pH and salt concentration on the surface potential of the $NH_2$-SAM. As discussed below, the differences in the surface potential with changing solution condition are due to the charging behavior at the PDMS–water interface. *Hy* is identical within error for all three salt concentrations (*Hy* = −0.20).

The analysis of the electrostatic forces indicates that the charging behavior of the PDMS interface is dramatically affected by the bulk pH. At pH ~10, the PDMS interface holds a large negative charge, resulting in an electrostatic repulsion with an opposing mica surface. The large negative charge at high pH is possibly due to adsorption of hydroxide ($OH^-$) and chloride ($Cl^-$) ions at the PDMS interface, which have recently been shown to adsorb at hydrophobic interfaces by multiple

**TABLE 2. Parameters for Modeling the Overall Interaction between PDMS Thin Films and Mica Surfaces at pH ~10[a]**

| [NaCl] (mM) | $\kappa^{-1}$ (nm) | $\kappa_{fit}^{-1}$ (nm) | $\psi_m$ (mV) | $\psi_P$ (mV) | *Hy* |
|---|---|---|---|---|---|
| 1 | 9.7 | 7 ± 0.5 | −80 ± 10 | −99 ± 21 | −0.20 ± 0.06 |
| 5 | 4.3 | 4.3 ± 0.5 | −100 ± 10 | −64 ± 15 | −0.20 ± 0.09 |
| 10 | 3.1 | 3.1 ± 0.5 | −105 ± 10 | −39 ± 6 | −0.20 ± 0.06 |

[a] The mica surface potential $\psi_m$ was measured in a separate experiment, and the Debye length ($\kappa^{-1}$) was calculated from the salt concentration, eq 4, except in the 1 mM case, which differed slightly from the expected theoretical value as indicated. The only fitting parameters were the PDMS surface potential ($\psi_P$) and *Hy*, which dominate at different length scales (Figure 5).

techniques.[37−41] While hydroxide ion adsorption seems to be the most likely explanation for the large negative charge measured here, no consensus has been reached and the issue remains controversial, from both experimental and theoretical perspectives.[42] Several experimental[38,39,43−47] and theoretical[39,48] studies have indeed found $OH^-$ adsorption at hydrophobic interfaces, while other experimental[49−51] and theoretical[52−54] papers determine that $OH^-$ is not surface active. We do not wish to stake a claim on either side of this argument. The experimental results unequivocally establish that the PDMS surface is negatively charged at high pH, although the identity and origin of ionic species at the interface are not directly measured in these experiments.

Alternate mechanisms for the negative charge at hydrophobic interfaces include (i) impurities that behave as surfactants resulting in the observed charge behavior,[50] although impurities seem unlikely in these experiments, or (ii) hydrogen-bonding asymmetry at hydrophobic interfaces.[55] Regardless, a large negative charge is clearly observed, especially at high pH, even as the nature of the charging remains unclear. At pH ~3, our SFA measurements indicate that the PDMS interface is effectively uncharged, a finding that further confirms literature reports that indicate that the isoelectric point of hydrophobic surfaces occurs at pH 3.[37−41]

It is interesting to note that the measured adhesion, corresponding to *Hy* values between 0.1 and 0.2, indicates that the mica is also behaving in a slightly hydrophobic manner at low pH. While still slightly charged, the charge has dramatically decreased, and an uncharged mica surface consists mainly of siloxane (Si−O−Si) linkages, which might be expected to be somewhat hydrophobic. Indeed, the control measurement between two mica surfaces (shown in Supporting Information) reveals an adhesion that appears to be larger than van der Waals forces between mica surfaces at low pH. This measurement confirms that mica is slightly hydrophobic at low pH, as was hinted in the earliest direct measurements between mica surfaces.[35] Our assertion that mica is slightly hydrophobic at pH ~3 is supported by recent pH-dependent contact angle measurements on mica surfaces, which showed a maximum contact angle of about 30° for a pH ~3 water

droplet, which progressively decreases to about 5° for pH ~12 water.[56] In fact, the large adhesion between mica surfaces at low pH, resulting in an adhesion energy over and above that expected by the vdW force, was observed already in 1973 (J. Israelachvili, unpublished data).

The observed PDMS surface potentials are in quantitative agreement with streaming potential measurements of PDMS[37,57] and AFM force measurements between silicone-oil-coated AFM tips and mica surfaces.[25,26] Further previous AFM work between hydrophobic and hydrophilic surfaces also captures similar trends: decreasing adhesion as one surface becomes more hydrophilic (or less hydrophobic),[21] and the observation that electrostatic models describe asymmetric hydrophobic−hydrophilic interactions remarkably well.[20]

Our results are also in qualitative agreement with several recent simulation studies. Wang *et al.*[58] examined competition between electrostatic and hydrophobic interactions by measuring binding affinity between a hydrophobic particle and hydrophobic plates of varying charge densities. They showed that for high charge densities the plate behaves as would be expected for a hydrophilic surface. As the charge density on the plate decreases, so does the apparent hydrophilicity, and hydrophobic behavior is recovered. Similarly, Patel *et al.*[59] studied dewetting transitions in biological molecules and showed that a drying transition can be triggered between two protein domains by turning the protein's partial charges off. When the partial charges are present, the protein interdomain regions remain wet. In principle, our results are analogous to both simulation studies: at high pH, the PDMS surface, while hydrophobic, displays no hydrophobic character because of the high charge density at the PDMS interface (Figure 5). At pH ~3, however, the PDMS interface is not charged and a weak hydrophobic attraction induces adhesion between the PDMS and mica interfaces.

## CONCLUSIONS

Click chemistry was used to devise the model silicone surface, which provides several advantages for designing model hydrophobic surfaces. The reaction selectively occurs at the interface, allowing for reliable and stable monolayer formation. No special reagents, techniques, or pieces of equipment are required, making the synthesis easy, adaptable, and consistent, resulting in smooth and hydrophobic surfaces. The ease of synthesis is especially advantageous for surface force measurements that require many square micrometers of clean and smooth surface area, and the stability of the surface allows for many measurements over the course of many hours or even multiple days. We have shown that formation of functional monolayers is easier and more reliable through selective and simple chemistry, leading to improved quality and functionality of the synthesized monolayers.

We postulate that *Hy* in general provides some *continuous* measure of the interfacial hydrophobicity/philicity and, by extension, the interfacial water structure, which has until now been lacking. Different hydrophobic and hydrophilic systems can now be classified based on *Hy*, thus providing a magnitude of the relative hydrophobic/philic interaction for a given system, and results can be compared to other techniques that more directly or locally measure the actual structuring of water. Molecular dynamics simulations have provided a fluctuating, vapor-like picture of hydrophobic interfaces. Focus now turns to examining if a relationship exists between the equilibrium hydrophobic surface force (measured by *Hy*) and the dynamic water structure near hydrophobic interfaces.

The quantitative meaning of the measured *Hy* values is somewhat unclear, because, as mentioned above, we have yet to derive a form for asymmetric hydrophobic−hydrophilic interactions. However, from a qualitative standpoint, the *Hy* values indicate a weak hydrophobic attraction between uncharged silicone and mica surfaces at low pH and a hydration repulsion due to adsorbed ions on both surfaces between charged silicone and mica surfaces at high pH. Thus, we have shown that simple pH adjustment leads to dramatically different ion adsorption behavior at hydrophobic surfaces and that *Hy* is correlated with this ion adsorption.

## METHODS

Surface forces measurements were performed at 21 °C with the SFA 2000 model, which has been described in detail elsewhere.[60] Briefly, the force ($F$) is measured as a function of distance ($D$) between the mica and gold surfaces. The distance between the surfaces and the contact mechanics are measured simultaneously by imaging the fringes of equal chromatic order. The asymmetric gold *vs* mica setup creates a two-layer interferometer, rather than the standard three-layer interferometer in usual mica *vs* mica SFA measurements.[61] The equations for the two-layer interferometer have been reported previously.[61] Molecularly smooth gold was prepared by templating with mica,[62] in which gold is evaporated onto freshly cleaved molecularly smooth mica. The gold is then glued onto a cylindrical silica disk with radius $R \approx 2$ cm, and immediately before each experiment, the mica was peeled off in ethanol, leaving behind a clean, molecularly smooth gold surface. Thin mica sheets were also glued onto disks, and gold and mica surfaces were mounted in the SFA in a cross-cylinder geometery for force and film thickness measurements. Before surface functionalization, clean gold and mica surfaces were brought into contact in the SFA to determine the reference mica−gold contact, *i.e.*, $D = 0$. During each force run, the distance was determined by capturing and analyzing the FECO fringes at a rate of 2 frames/second. The surfaces were approached and separated at a slow (quasi-static) rate (*e.g.*, 2 nm/s) in the noninteracting regime, and variation from this rate within the interacting regime is due to deflection of a cantilevered spring, allowing for determination of the interaction force. As mentioned previously, a jump (mechanical instability) occurs when

the gradient of the force profile is larger than the spring constant; these dynamic jumps into or out of contact are shown by displaying arrows on the force curves.

Silicone thin films were prepared by the following grafting procedure. After cleaving the mica away, the clean gold surface was rinsed with ethanol and immediately immersed in a 1 mM ethanolic solution of 11-amino-1-undecanethiol hydrochloride (Sigma-Aldrich) for 2 h. Two drops of triethylamine were added to this solution to prevent oxidation of the amine groups. The reaction was done in a dark room (to avoid photo-oxidation of the monolayer) at 21 °C. Following the 2 h period, the surface was rinsed extensively with ethanol and blown dry with nitrogen gas, leaving behind a single monolayer of amino-terminated thiol on gold. After drying, the surface was immediately immersed in pure monoglycidyl ether-terminated PDMS liquid ($M_n$ = 5000 g/mol, Sigma-Aldrich) and placed in the oven at 130 °C for 1 h. The reaction proceeds as described above and results in a monolayer of covalently attached PDMS molecules.

An extensive cleaning procedure was employed to remove physically bound PDMS molecules. The surface is first rinsed with ethanol, followed by extensive rinsing in toluene. PDMS is soluble in toluene, so any physisorbed molecules should be removed in the toluene rinses. After rinsing in toluene, the surface is immersed in toluene and sonicated. A total of three rinse/sonication cycles were done. Care must be taken during sonication, because excessive sonication can damage the gold surface and render it useless for the surface forces measurements. Thus, the sonication time was progressively decreased; that is, the first sonication was for 15 s, followed by 10 s, and finally 5 s for the third and final sonication step. Longer sonication times result in a greater amount of small asperities, as observed by FECO, which are induced by the sonication. Several early experiments were ruined by the presence of asperities before the cleaning/sonication procedure was refined. All reported SFA force runs and film thickness measurements were performed at clean, smooth, asperity-free contact zones. After the sonication/rinse cycles, the surface was rinsed again with toluene and finally with ethanol and immersed in ethanol for a short time (generally less than 20 min) before installing into the SFA and starting the force measurements.

After rinsing with ethanol and blow-drying with nitrogen gas, the PDMS-on-gold surface was installed into the SFA along with a clean mica surface in cross-cylinder geometry. The apparatus was filled with the NaCl solution, and all solutions were degassed by stirring with Teflon chips and pulling a weak vacuum for at least 1 h before transferring to the SFA. The pH was adjusted by adding HCl or NaOH and not buffered, resulting in some pH variability. The actual pH varied up to $\pm$0.3 pH units. Thus, references to pH $\sim$3 here correspond to actual pH = 3 $\pm$ 0.1, while references to pH $\sim$10 correspond to actual pH = 10 $\pm$ 0.3.

The SFA results are representative for at least 10 different experimental setups. In a single experimental setup, the distance accuracy is about $\pm$2.5 Å and the *F*/*R* resolution is about 0.1 mN/m. However, variability in the synthesized monolayers and mica surfaces results in significant uncertainty in the measured potentials and parameters shown in Tables 1 and 2. The error bars in those cases are the standard deviation over the entire data set and represent variability due to natural variability of the mica surfaces, as well as the synthetic variability due to quality of reagents (which can change over time, especially for thiols) and environmental factors.

Contact angle measurements were performed with a home-built goniometer, equipped with a camera and a syringe pump. The results presented are representative of five independent monolayer preparations and at least three separate contact positions on each surface. Measurements were done by advancing and receding a 5 $\mu$L droplet of pure water on the silicone layer at a rate of 1 $\mu$L/min. The angles were analyzed with the ImageJ contact angle plugin using the ellipsoid fitting routine.

X-ray photoelectron spectra were measured using a Kratos Axis Ultra system with a monochromated Al K$\alpha$ source (1486.6 eV, 225 W). An electron flood gun was used for charge neutralization to compensate for the nonconducting samples. All spectra were referenced to the Au 4f signal for bulk gold (84 eV). For all spectra, a linear baseline correction was used for all three samples in a given energy range in order to subtract the background intensity.

*Conflict of Interest:* The authors declare no competing financial interest.

*Supporting Information Available:* AFM imaging of PDMS thin film; XPS spectral deconvolution; SFA measurements between mica surfaces; calculation of van der Waals forces between PDMS thin films and mica surfaces; SFA measurements between mica surfaces and hydrophobic alkanethiol monolayers. This material is available free of charge *via* the Internet at http://pubs.acs.org.

*Acknowledgment.* This work was supported by a gift from the Procter & Gamble Company, *via* a collaboration led jointly by Dr. Gizaw, Dr. Koenig, and Dr. Bruce Murch. XPS measurements were conducted in the MRL Shared Experimental Facilities. The MRL Shared Experimental Facilities are supported by the MRSEC Program of the NSF under Award No. DMR 1121053, a member of the NSF-funded Materials Research Facilities Network (www.mrfn.org). We would also like to thank Dr. Sumanth Jamadagni for useful discussions.

## REFERENCES AND NOTES

1. Bongaerts, J. H. H.; Fourtouni, K.; Stokes, J. R. Soft-Tribology: Lubrication in a Compliant PDMS-PDMS Contact. *Tribol. Int.* **2007**, *40*, 1531–1542.
2. Lee, S.; Spencer, N. D. Aqueous Lubrication of Polymers: Influence of Surface Modification. *Tribol. Int.* **2005**, *38*, 922–930.
3. Duffy, D. C.; McDonald, J. C.; Schueller, O. J. A.; Whitesides, G. M. Rapid Prototyping of Microfluidic Systems in Poly(dimethylsiloxane). *Anal. Chem.* **1998**, *70*, 4974–4984.
4. McDonald, J. C.; Duffy, D. C.; Anderson, J. R.; Chiu, D. T.; Wu, H. K.; Schueller, O. J. A.; Whitesides, G. M. Fabrication of Microfluidic Systems in Poly(dimethylsiloxane). *Electrophoresis* **2000**, *21*, 27–40.
5. McDonald, J. C.; Whitesides, G. M. Poly(dimethylsiloxane) as a Material for Fabricating Microfluidic Devices. *Acc. Chem. Res.* **2002**, *35*, 491–499.
6. Sia, S. K.; Whitesides, G. M. Microfluidic Devices Fabricated in Poly(dimethylsiloxane) for Biological Studies. *Electrophoresis* **2003**, *24*, 3563–3576.
7. Khademhosseini, A.; Langer, R.; Borenstein, J.; Vacanti, J. P. Microscale Technologies for Tissue Engineering and Biology. *Proc. Natl. Acad. Sci. U.S.A.* **2006**, *103*, 2480–2487.
8. Williams, D. F. On the Mechanisms of Biocompatibility. *Biomaterials* **2008**, *29*, 2941–2953.
9. Binks, B. P.; Whitby, C. P. Silica Particle-Stabilized Emulsions of Silicone Oil and Water: Aspects of Emulsification. *Langmuir* **2004**, *20*, 1130–1137.
10. Zhu, X. M.; Fryd, M. M.; Huang, J. R.; Mason, T. G. Optically Probing Nanoemulsion Compositions. *Phys. Chem. Chem. Phys.* **2012**, *14*, 2455–2461.
11. Kim, J.; Gao, Y. X.; Hebebrand, C.; Peirtsegaele, E.; Helgeson, M. E. Polymer-Surfactant Complexation as a Generic Route to Responsive Viscoelastic Nanoemulsions. *Soft Matter* **2013**, *9*, 6897–6910.
12. Hu, S. W.; Ren, X. Q.; Bachman, M.; Sims, C. E.; Li, G. P.; Allbritton, N. Surface Modification of Poly(dimethylsiloxane) Microfluidic Devices by Ultraviolet Polymer Grafting. *Anal. Chem.* **2002**, *74*, 4117–4123.
13. Liu, D. J.; Perdue, R. K.; Sun, L.; Crooks, R. M. Immobilization of DNA onto Poly(dimethylsiloxane) Surfaces and Application to a Microelectrochemical Enzyme-Amplified DNA Hybridization Assay. *Langmuir* **2004**, *20*, 5905–5910.
14. Toepke, M. W.; Beebe, D. J. PDMS Absorption of Small Molecules and Consequences in Microfluidic Applications. *Lab Chip* **2006**, *6*, 1484–1486.
15. Kolb, H. C.; Finn, M. G.; Sharpless, K. B. Click Chemistry: Diverse Chemical Function from a Few Good Reactions. *Angew. Chem., Int. Ed.* **2001**, *40*, 2004–2021.
16. Moses, J. E.; Moorhouse, A. D. The Growing Applications of Click Chemistry. *Chem. Soc. Rev.* **2007**, *36*, 1249–1262.

17. Chelmowski, R.; Koester, S. D.; Kerstan, A.; Prekelt, A.; Grunwald, C.; Winkler, T.; Metzler-Nolte, N.; Terfort, A.; Woell, C. Peptide-Based SAMs That Resist the Adsorption of Proteins. *J. Am. Chem. Soc.* **2008**, *130*, 14952–14953.
18. Hudalla, G. A.; Murphy, W. L. Using "Click" Chemistry to Prepare SAM Substrates to Study Stem Cell Adhesion. *Langmuir* **2009**, *25*, 5737–5746.
19. Decreau, R. A.; Collman, J. P.; Hosseini, A. Electrochemical Applications. How Click Chemistry Brought Biomimetic Models to the Next Level: Electrocatalysis under Controlled Rate of Electron Transfer. *Chem. Soc. Rev.* **2010**, *39*, 1291–1301.
20. Kokkoli, E.; Zukoski, C. F. Interaction Forces between Hydrophobic and Hydrophilic Self-Assembled Monolayers. *J. Colloid Interface Sci.* **2000**, *230*, 176–180.
21. Yoon, R. H.; Flinn, D. H.; Rabinovich, Y. I. Hydrophobic Interactions between Dissimilar Surfaces. *J. Colloid Interface Sci.* **1997**, *185*, 363–370.
22. Meyer, E. E.; Rosenberg, K. J.; Israelachvili, J. Recent Progress in Understanding Hydrophobic Interactions. *Proc. Natl. Acad. Sci. U.S.A.* **2006**, *103*, 15739–15746.
23. Liberelle, B.; Giasson, S. Chemical End-Grafting of Homogeneous Polystyrene Monolayers on Mica and Silica Surfaces. *Langmuir* **2007**, *23*, 9263–9270.
24. Liberelle, B.; Giasson, S. Friction and Normal Interaction Forces between Irreversibly Attached Weakly Charged Polymer Brushes. *Langmuir* **2008**, *24*, 1550–1559.
25. Zbik, M. S.; Frost, R. L. Afm Study of Forces between Silicon Oil and Hydrophobic-Hydrophilic Surfaces in Aqueous Solutions. *J. Colloid Interface Sci.* **2010**, *349*, 492–497.
26. Kumar, D.; Biswas, S. K. Contribution of Different Physical Forces to the Disjoining Pressure of a Thin Water Film Being Pressed by an Oil Droplet. *J. Colloid Interface Sci.* **2010**, *348*, 255–264.
27. Degennes, P. G. Conformations of Polymers Attached to an Interface. *Macromolecules* **1980**, *13*, 1069–1075.
28. Halperin, A. Collapse of Grafted Chains in Poor Solvents. *J. Phys. (Paris)* **1988**, *49*, 547–550.
29. Moh, L. C. H.; Losego, M. D.; Braun, P. V. Solvent Quality Effects on Scaling Behavior of Poly(methyl methacrylate) Brushes in the Moderate- and High-Density Regimes. *Langmuir* **2011**, *27*, 3698–3702.
30. Scales, P. J.; Grieser, F.; Healy, T. W. Electrokinetics of the Muscovite Mica Aqueous-Solution Interface. *Langmuir* **1990**, *6*, 582–589.
31. Nishimura, S.; Tateyama, H.; Tsunematsu, K.; Jinnai, K. Zeta-Potential Measurement of Muscovite Mica Basal-Plane Aqueous-Solution Interface by Means of Plane Interface Technique. *J. Colloid Interface Sci.* **1992**, *152*, 359–367.
32. Donaldson, S. H.; Lee, C. T.; Chmelka, B. F.; Israelachvili, J. N. General Hydrophobic Interaction Potential for Surfactant/Lipid Bilayers from Direct Force Measurements between Light-Modulated Bilayers. *Proc. Natl. Acad. Sci. U.S.A.* **2011**, *108*, 15699–15704.
33. Sanchez-Iglesias, A.; Grzelczak, M.; Altantzis, T.; Goris, B.; Perez-Juste, J.; Bals, S.; Van Tendeloo, G.; Donaldson, S. H.; Chmelka, B. F.; Israelachvili, J. N.; *et al*. Hydrophobic Interactions Modulate Self-Assembly of Nanoparticles. *ACS Nano* **2012**, *6*, 11059–11065.
34. Israelachvili, J.; Wennerstrom, H. Role of Hydration and Water Structure in Biological and Colloidal Interactions. *Nature* **1996**, *379*, 219–225.
35. Israelachvili, J. N.; Adams, G. E. Measurement of Forces between 2 Mica Surfaces in Aqueous-Electrolyte Solutions in Range 0−100 Nm. *J. Chem. Soc., Faraday Trans. 1* **1978**, *74*, 975–1001.
36. Israelachvili, J. *Intermolecular and Surface Forces*, 3rd ed.; Elsevier, 2011.
37. Beattie, J. K. The Intrinsic Charge on Hydrophobic Microfluidic Substrates. *Lab Chip* **2006**, *6*, 1409–1411.
38. Tian, C. S.; Shen, Y. R. Structure and Charging of Hydrophobic Material/Water Interfaces Studied by Phase-Sensitive Sum-Frequency Vibrational Spectroscopy. *Proc. Natl. Acad. Sci. U.S.A.* **2009**, *106*, 15148–15153.
39. Mishra, H.; Enami, S.; Nielsen, R. J.; Stewart, L. A.; Hoffmann, M. R.; Goddard, W. A., III; Colussi, A. J. Bronsted Basicity of the Air-Water Interface. *Proc. Natl. Acad. Sci. U.S.A.* **2012**, *109*, 18679–18683.
40. Creux, P.; Lachaise, J.; Graciaa, A.; Beattie, J. K.; Djerdjev, A. M. Strong Specific Hydroxide Ion Binding at the Pristine Oil/Water and Air/Water Interfaces. *J. Phys. Chem. B* **2009**, *113*, 14146–14150.
41. Preocanin, T.; Selmani, A.; Lindqvist-Reis, P.; Heberling, F.; Kallay, N.; Luetzenkirchen, J. Surface Charge at Teflon/Aqueous Solution of Potassium Chloride Interfaces. *Colloid Surf. A: Physicochem. Eng. Asp.* **2012**, *412*, 120–128.
42. Saykally, R. J. Air/Water Interface Two Sides of the Acid-Base Story. *Nat. Chem.* **2013**, *5*, 82–84.
43. Beattie, J. K.; Djerdjev, A. N.; Warr, G. G. The Surface of Neat Water Is Basic. *Faraday Discuss.* **2009**, *141*, 31–39.
44. Marinova, K. G.; Alargova, R. G.; Denkov, N. D.; Velev, O. D.; Petsev, D. N.; Ivanov, I. B.; Borwankar, R. P. Charging of Oil-Water Interfaces Due to Spontaneous Adsorption of Hydroxyl Ions. *Langmuir* **1996**, *12*, 2045–2051.
45. Gray-Weale, A.; Beattie, J. K. An Explanation for the Charge on Water's Surface. *Phys. Chem. Chem. Phys.* **2009**, *11*, 10994–11005.
46. Beattie, J. K.; Gray-Weale, A. Oil/Water Interface Charged by Hydroxide Ions and Deprotonated Fatty Acids: A Comment. *Angew. Chem., Int. Ed.* **2012**, *51*, 12941–12942.
47. Jena, K. C.; Scheu, R.; Roke, S. Surface Impurities Are Not Responsible for the Charge on the Oil/Water Interface: A Comment. *Angew. Chem., Int. Ed.* **2012**, *51*, 12938–12940.
48. Zangi, R.; Engberts, J. Physisorption of Hydroxide Ions from Aqueous Solution to a Hydrophobic Surface. *J. Am. Chem. Soc.* **2005**, *127*, 2272–2276.
49. Petersen, P. B.; Saykally, R. J. Is the Liquid Water Surface Basic or Acidic? Macroscopic vs. Molecular-Scale Investigations. *Chem. Phys. Lett.* **2008**, *458*, 255–261.
50. Roger, K.; Cabane, B. Why Are Hydrophobic/Water Interfaces Negatively Charged? *Angew. Chem., Int. Ed.* **2012**, *51*, 5625–5628.
51. Roger, K.; Cabane, B. Uncontaminated Hydrophobic/Water Interfaces Are Uncharged: A Reply. *Angew. Chem., Int. Ed.* **2012**, *51*, 12943–12945.
52. Buch, V.; Milet, A.; Vacha, R.; Jungwirth, P.; Devlin, J. P. Water Surface Is Acidic. *Proc. Natl. Acad. Sci. U.S.A.* **2007**, *104*, 7342–7347.
53. Vacha, R.; Buch, V.; Milet, A.; Devlin, P.; Jungwirth, P. Autoionization at the Surface of Neat Water: Is the Top Layer pH Neutral, Basic, or Acidic? *Phys. Chem. Chem. Phys.* **2007**, *9*, 4736–4747.
54. Iuchi, S.; Chen, H.; Paesani, F.; Voth, G. A. Hydrated Excess Proton at Water-Hydrophobic Interfaces. *J. Phys. Chem. B* **2009**, *113*, 4017–4030.
55. Vacha, R.; Rick, S. W.; Jungwirth, P.; de Beer, A. G. F.; de Aguiar, H. B.; Samson, J.-S.; Roke, S. The Orientation and Charge of Water at the Hydrophobic Oil Droplet-Water Interface. *J. Am. Chem. Soc.* **2011**, *133*, 10204–10210.
56. Horiuchi, H.; Nikolov, A.; Wasan, D. T. Calculation of the Surface Potential and Surface Charge Density by Measurement of the Three-Phase Contact Angle. *J. Colloid Interface Sci.* **2012**, *385*, 218–224.
57. Kirby, B. J.; Hasselbrink, E. F. Zeta Potential of Microfluidic Substrates: 2. Data for Polymers. *Electrophoresis* **2004**, *25*, 203–213.
58. Wang, L.; Friesner, R. A.; Berne, B. J. Competition of Electrostatic and Hydrophobic Interactions between Small Hydrophobes and Model Enclosures. *J. Phys. Chem. B* **2010**, *114*, 7294–7301.
59. Patel, A. J.; Varilly, P.; Jamadagni, S. N.; Hagan, M. F.; Chandler, D.; Garde, S. Sitting at the Edge: How Biomolecules Use Hydrophobicity to Tune Their Interactions and Function. *J. Phys. Chem. B* **2012**, *116*, 2498–2503.
60. Israelachvili, J.; Min, Y.; Akbulut, M.; Alig, A.; Carver, G.; Greene, W.; Kristiansen, K.; Meyer, E.; Pesika, N.; Rosenberg, K.; *et al*. Recent Advances in the Surface Forces Apparatus (SFA) Technique. *Rep. Prog. Phys.* **2010**, *73*, 036601.

61. Israelachvili, J. Thin-Film Studies Using Multiple-Beam Interferometry. *J. Colloid Interface Sci.* **1973**, *44*, 259–272.
62. Chai, L.; Klein, J. Large Area, Molecularly Smooth (0.2 nm rms) Gold Films for Surface Forces and Other Studies. *Langmuir* **2007**, *23*, 7777–7783.